# Adsorption of bitumen model compounds on kaolinite in liquid and supercritical carbon dioxide solvents: a study by periodic density functional theory and molecular theory of solvation

Ribeiro Lage, Mateus; Stoyanov, Stanislav R.; de Mesquita Carneiro, José Walkimar; Dabros, Tadek; Kovalenko, Andriy



**Publisher's version / Version de l'éditeur:**
https://doi.org/10.1021/ef502202q
*Energy & Fuels, 29, 5, pp. 2853-2863, 2015-05-21*

energy&fuels

Article

pubs.acs.org/EF

# Adsorption of Bitumen Model Compounds on Kaolinite in Liquid and Supercritical Carbon Dioxide Solvents: A Study by Periodic Density Functional Theory and Molecular Theory of Solvation

Mateus Ribeiro Lage,[†,‡,§] Stanislav R. Stoyanov,[*,†,§,∥,⊥] José Walkimar de Mesquita Carneiro,[*,‡] Tadek Dabros,[*,∥,⊥] and Andriy Kovalenko[*,†,§]

[†]National Institute for Nanotechnology, 11421 Saskatchewan Drive Northwest, Edmonton, Alberta T6G 2M9, Canada

[‡]Department of Inorganic Chemistry, Fluminense Federal University, Outeiro de São João Batista, s/n, Centro, 24020-141 Niterói, Rio de Janeiro, Brazil

[§]Department of Mechanical Engineering, University of Alberta, Edmonton Alberta T6G 2G3, Canada

[∥]Canmet Energy Technology Centre, Natural Resources Canada, 1 Oil Patch Drive, Devon, Alberta T9G 1A8, Canada

[⊥]Department of Chemical and Materials Engineering, University of Alberta, Edmonton, Alberta T6G 2V4, Canada

*Supporting Information*

**ABSTRACT:** The geometry of phenanthridine, benzothiophene, tetralin, and naphthalene representative of the heterocyclic, naphthenic, and aromatic components of bitumen adsorbed on kaolinite is optimized using density functional theory and periodic boundary conditions in gas phase. These bitumen model compounds preferentially adsorb on the aluminum hydroxide surface of kaolinite with energy decreasing in the order phenanthridine > naphthalene > tetralin ∼ benzothiophene. The adsorption of phenanthridine is strengthened by hydrogen bonding between the pyridinic N atom and an axial hydroxyl group of kaolinite, while the rest of the molecules adsorb through van der Waals interactions. The mechanism of solvation in $CO_2$ and the effect of liquid and supercritical $CO_2$ on the adsorption thermodynamics are studied using the three-dimensional reference interaction site model theory with the closure approximation of Kovalenko and Hirata (3D-RISM-KH) molecular theory of solvation at 293−333 K and 10−30 MPa. The $CO_2$ solvent interacts with the aluminum hydroxide surface of kaolinite by hydrogen bonding, with the pyridinic N atom of phenanthridine by electrostatic interactions, and with the rest of the bitumen model compounds by hydrophobic interactions, as inferred from the 3D site density distribution functions of $CO_2$. The molecule−kaolinite potentials of mean force in $CO_2$ show that the adsorption of naphthalene and tetralin on kaolinite is substantially weakened as the pressure is increased and the temperature is decreased. Benzothiophene adsorption is the least sensitive to $CO_2$ temperature and pressure changes. In liquid $CO_2$ at 30 MPa and 293 K, the hydrocarbon molecules are weakly adsorbed and can be desorbed by $CO_2$, while the heterocycles would remain adsorbed, suggesting an approach for extraction of deasphalted bitumen from oil sands. While the most favorable thermodynamic conditions for desorption are in liquid $CO_2$, the kinetic barrier for desorption is the most sensitive to small changes in the temperature and pressure in supercritical $CO_2$, indicating that supercritical conditions are important for desorption rate control. These results suggest that the investigated bitumen components can be selectively desorbed from kaolinite by controlling the temperature and pressure of the $CO_2$ solvent and agree with experimental reports on heavy oil recovery. These insights are valuable for the development of improved techniques for extraction of bitumen from oil sands and deasphalting of bitumen using liquid and supercritical $CO_2$.

## INTRODUCTION

Canada's oil sands hold the third largest petroleum reserve in the world.[1] The main challenge in the development of this valuable resource is that oil sands contain typically 7−12% of hydrocarbons in the form of bitumen, a very heavy petroleum, mixed with sand, clays, and several percent water. Bitumen-rich oil sands are mined in open surface mines, if available near the surface. When buried deep, bitumen is extracted *in situ*, mainly using the steam-assisted gravity drainage (SAGD) technique.[2] Extraction of bitumen from surface-mined oil sands using hot water (sometimes with additives) by the Karl Clark method is currently the predominant technology employed to produce ∼2 million barrels of synthetic crude oil per day in Alberta.[3,4] This is a costly and carbon-intense process that requires large amounts of water. Non-aqueous bitumen extraction is an important alternative to hot-water extraction. Several approaches for extraction of bitumen using critical/supercritical $CO_2$,[5] ionic liquids at close to ambient conditions,[6] organic solvents,[7−9] and hybrid aqueous−non-aqueous processes[10] have been tested at small scale.[7,11]

Carbon dioxide is a nonpolar molecule with a relatively large quadrupole moment ($13.4 \times 10^{-40}$ C m$^2$)[12] compared to 0, $3.34 \times 10^{-40}$, $5.00 \times 10^{-40}$, and $4.7 \times 10^{-40}$ C m$^2$ for methane, ethane, ethylene, and $N_2$, respectively.[13,14] It is this large

**Special Issue:** 15th International Conference on Petroleum Phase Behavior and Fouling

**Received:** September 19, 2014
**Revised:** December 15, 2014
**Published:** December 26, 2014





DOI: 10.1021/ef502202q
*Energy Fuels* 2015, 29, 2853−2863

quadrupole moment that makes the phase behavior of supercritical $CO_2$ much more challenging to predict than that of other nonpolar fluids.[15] An important consequence of the quadrupole moment is that $CO_2$ can act as a Lewis acid (C atom) and a Lewis base (O atoms).[16] Also, the O atoms can be involved in weak electrostatic interactions, such as weak hydrogen bonds and cooperative C−H···O bonds.[17−19] These chemical interactions largely determine the successful applications of dense $CO_2$ in enhanced oil recovery[20,21] and vacuum residual treatment.[22−25]

Supercritical $CO_2$ is becoming an important extraction solvent in chemical engineering processes, such as decaffeination of coffee[26] and enhanced oil recovery,[20,21] because of the enhanced and tunable solubility of organic compounds in this solvent. Supercritical $CO_2$ is particularly attractive for being a nontoxic and nonflammable solvent with low viscosity, high diffusion rate, and no surface tension. Moreover, the relatively low critical parameters ($T_c$ = 304.1 K, and $P_c$ = 7.39 MPa) as well as a very low cost make it feasible not to recycle supercritical $CO_2$. The main drawback of supercritical $CO_2$-based extraction is that only volatile and nonpolar compounds are soluble in it.[27] The solvation strength of supercritical $CO_2$ is related to its dielectric constant and density. The dielectric constant of supercritical $CO_2$ ranges from 1.12 at 353 K and 10 MPa (density of 0.22 g/cm$^3$) to 1.58 at 305 K and 30 MPa (density of 0.94 g/cm$^3$), and in liquid $CO_2$, it reaches 1.67 at 273 K and 30 MPa (density of 1.05 g/cm$^3$).[28] From these dielectric constant values, supercritical $CO_2$ is classified as a nonpolar solvent, comparable to *n*-hexane.[29] The most attractive temperature and pressure ranges for extraction in $CO_2$ are 303−333 K and 10−30 MPa, respectively, because in this part of the $CO_2$ phase diagram, it is possible to tune solubility over a wide range with either a small isobaric temperature change or a small isothermic pressure change.

Oil extraction from natural oil sands and soil samples has been studied experimentally to determine the optimal $CO_2$ solvent conditions.[30−32] It is challenging to interpret these results at a mechanistic chemistry level because of the diversity of natural samples, role of soaking,[31] and multiple stages of extraction, e.g., desorption from solid grain, intraparticle diffusion, and transfer of oil into the bulk fluid.[32] Recent reports highlight the necessity to investigate the effect of the $CO_2$ temperature and pressure on the extraction of individual oil components, such as aromatics, aliphatics, and naphthenes,[30] and the destiny of asphaltenes.[33]

The mechanism of interaction of $CO_2$ with organic molecules and clay minerals has been investigated using electronic structure methods and molecular dynamics simulations. The interaction of amines with $CO_2$ and the relative energies of the zwitterion intermediates in the carbamic acid reaction mechanism have been studied using pure and hybrid density functionals.[34,35] Correlated *ab initio* molecular dynamics simulations of the acetone−$CO_2$ complex reveal the Lewis acid and Lewis base behaviors of $CO_2$.[36] Density functional theory (DFT) studies of the condensation of supercritical $CO_2$ on kaolinite agree with microbalance measurements in that $CO_2$ adsorption is favorable and shows distorted T-shaped clustering.[37] The adsorption of hydrocarbons and heterocycles on kaolinite have also been studied using the exchange hole dipole moment dispersion model.[38] Molecular dynamics simulations have been employed to study the solvation of model petroleum asphaltenes[39] and intercalation of $CO_2$ into montmorillonite in supercritical $CO_2$.[40,41] The molecular interactions among supercritical $CO_2$, brine, and kaolinite have been studied using large-scale molecular dynamics to determine the contact angle of $CO_2$ droplets.[42]

An important alternative to molecular simulations, the three-dimensional reference interaction site model theory with the closure approximation of Kovalenko and Hirata (3D-RISM−KH), predicts successfully solvation in complex molecular nanosystems based on the first principles of statistical mechanics.[43−48] The 3D-RISM−KH molecular theory of solvation properly accounts for hydrophobic and hydrogen-bonding interactions and reproduces structural and phase transitions in simple and complex liquids and solutions in a wide range of thermodynamic conditions[49,50] and in nanoporous confinement.[51−54] The 3D-RISM−KH theory has been employed to predict the solvation structure and thermodynamics of electrolyte solutions[45,46] and ionic liquids,[55] gelation activity,[56,57] molecular boundary conditions of hydrodynamic flow,[58] self-assembly and conformational transitions of synthetic organic supramolecular rosette nanotubular architectures,[59,60] molecular recognition in biomolecular nanostystems,[61,62] and nanoscale forces in plant cell walls.[63] In heavy oil research, the 3D-RISM−KH theory has been employed to study the adsorption of thiophenic heterocycles on ion-exchanged zeolite surfaces in the presence of a benzene solvent[64] as well as for prediction of the effect of the temperature on asphaltene aggregation in quinoline and 1-methylnaphthalene solvents.[65] The effect of trace amounts of water in a chloroform solvent on the free energy of aggregation of model asphaltene compounds containing polyaromatic hydrocarbon moieties tethered to pyridyl groups has been investigated using the 3D-RISM−KH theory, and the contributions of hydrogen-bonding and $\pi-\pi$ stacking interactions to aggregation are evaluated on the basis of electronic structure calculations.[66,67]

Recently, we have reported on a 3D-RISM−KH investigation of the adsorption of indole on kaolinite and presented insights into its preferred adsorption orientation and effective interaction potential for adsorption in heptane and toluene solvents. The calculated multilayer adsorption profiles have been correlated with experimentally determined monolayer and saturation loading of organoclays driven by strong adsorbate−adsorbate interactions.[68] The molecular recognition interactions of S- and N-containing heterocycles (relevant to asphaltenes) toward kaolinite have been investigated in a toluene solvent using the 3D-RISM−KH method to gain insight into this entropy-driven organization and correlated with experimental adsorption kinetic and thermodynamic studies.[69]

In the present work, we study the adsorption of model bitumen compounds on kaolinite using the PW91 density functional and periodic boundary conditions (PBC). The mechanism of solvation of systems containing kaolinite platelet and bitumen molecules in a $CO_2$ solvent is explored using the 3D-RISM−KH molecular theory of solvation. Moreover, the effect of the temperature and pressure of $CO_2$ on the thermodynamics of adsorption of bitumen components on kaolinite is investigated to gain insight relevant to extraction of bitumen from oil sands and deasphalting.

## ■ COMPUTATIONAL TECHNIQUE

**Geometry Optimization Using DFT in PBC.** The geometry of phenanthridine, benzothiophene, naphthalene, and tetralin (panels a−d of Scheme 1) on kaolinite (Scheme 1e) are optimized in PBC using


DOI: 10.1021/ef502202q
*Energy Fuels* 2015, 29, 2853−2863

**Scheme 1. Chemical Structures of (a) Phenanthridine, (b) Benzothiophene, (c) Tetralin, (d) Naphthalene, and (e) Kaolinite Surface Unit Showing Axes Orientation**

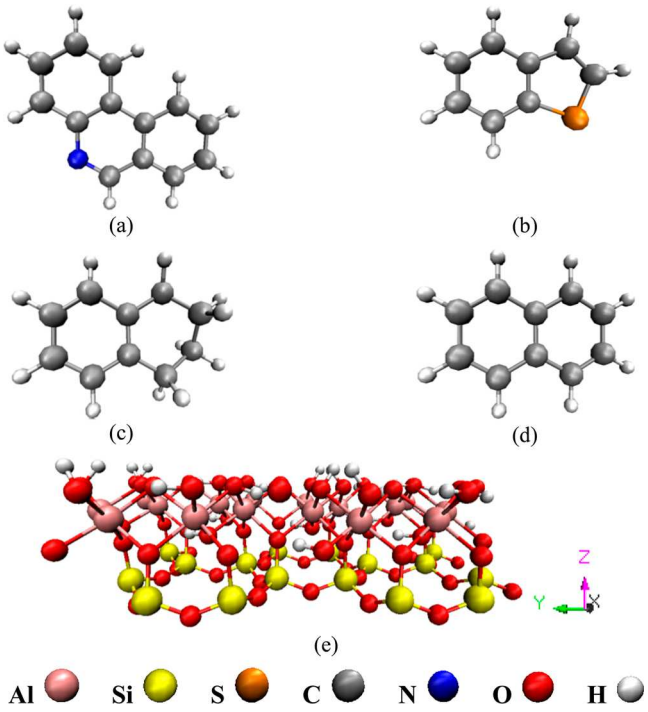


the functional by Perdew and Wang (PW91)[70] and double numerical basis set with polarization function for H atom (DNP),[71] as implemented in the DMol$^3$ module of the Accelrys Materials Studio software suite.[72] The kaolinite surface is represented as a single sheet with dimensions A2 × B1 placed in a 10.30 × 8.93 × 64.00 A$^3$ periodic cell[73] to allow for a 56.6 Å vacuum slab along the $z$ axis. Thus, kaolinite is modeled as a continuous surface without edge termination effects. The molecules are placed near the aluminum hydroxide surface in three initial orientations at angles of 0°, 45°, and 90° relative to the $xy$ plane defined in Scheme 1e, and the positions of all atoms of kaolinite and molecule are optimized.

The PW91 functional was selected because it yields optimized geometries that are in better agreement with the experiment than those from other functionals, such as the widely used B3LYP functional.[74,75] It has also been shown that PW91 is capable of modeling van der Waals interactions, although it has not been specifically built to describe dispersive interactions.[76] Brillouin zone sampling is restricted to the Γ point. An extrafine numerical integration grid that contains 474 angular points is used. The DMol$^3$ numerical frequency analysis is applied to confirm that the optimized structures are true minima in the potential energy surface. This computational approach has been validated and employed to study the adsorption of bitumen components on the surface of the zeolite chabazite.[77]

**1D/3D-RISM−KH Theory Overview.** The 3D-RISM−KH molecular theory of solvation couples the 3D-RISM integral equation for 3D solute−solvent site correlation functions[78,79] (eq 1) with the 3D version of the Kovalenko−Hirata (KH) closure approximation (eq 2), as follows:

$$h_\gamma(\mathbf{r}) = \sum_{\gamma'} \int \mathrm{d}\mathbf{r}' c_{\gamma'}(\mathbf{r}')\chi_{\gamma'\gamma}(|\mathbf{r} - \mathbf{r}'|) \tag{1}$$

$$g_\gamma(\mathbf{r}) = \begin{cases} \exp(d_\gamma(\mathbf{r})) & \text{for} \quad d_\gamma(\mathbf{r}) \le 0 \\ 1 + d_\gamma(\mathbf{r}) & \text{for} \quad d_\gamma(\mathbf{r}) > 0 \end{cases} \tag{2}$$

$$d_\gamma(\mathbf{r}) = \frac{u_\gamma(\mathbf{r})}{k_\mathrm{B}T} + h_\gamma(\mathbf{r}) - c_\gamma(\mathbf{r})$$

where $h_\gamma(\mathbf{r})$ and $c_\gamma(\mathbf{r})$ are the 3D total and direct correlation functions of solvent site $\gamma$ around the solute, respectively, $\chi_{\gamma'\gamma}(\mathbf{r})$ is the site−site susceptibility of the solvent, which is calculated beforehand, and indices $\alpha$ and $\gamma$ enumerate all interaction sites on all sorts of solvent species. The 3D distribution function (normalized density distribution) of solvent site $\gamma$ is $g_\gamma(\mathbf{r})$ and is related with $h_\gamma(\mathbf{r})$ as $g_\gamma(\mathbf{r}) = h_\gamma(\mathbf{r}) + 1$. A $g_\gamma(\mathbf{r})$ value of 1.0 corresponds to bulk solvent distribution far from the solute. When $g_\gamma(\mathbf{r}) > 1.0$, the solvent site density is enhanced relative to the bulk solvent. When $g_\gamma(\mathbf{r}) < 1.0$, the solvent density is depleted relative to the bulk solvent. The 3D interaction potential $u_\gamma(\mathbf{r})$ between the whole solute and solvent site $\gamma$ is specified by a molecular force field, and $k_\mathrm{B}T$ is the Boltzmann constant times the solution temperature.[43−46] The total correlation function $h_\gamma(\mathbf{r})$ has the physical meaning of a normalized 3D distribution of spatial correlations or normalized deviations of solvent site local density around the solute molecule from its average value of the solvent site number density $\rho_\gamma$ in the solution bulk.

The site−site susceptibility of solvent $\chi_{\alpha\gamma}(r)$ determines the nonlocal response of the solvent to the insertion of the solute macromolecule propagating across the solvation shells. It breaks up into the intra- and intermolecular terms as $\chi_{\alpha\gamma}(r) = \omega_{\alpha\gamma}(r) + \rho_\alpha h_{\alpha\gamma}(r)$. The intramolecular correlation function $\omega_{\alpha\gamma}(r)$ normalized as $\int \mathrm{d}\mathbf{r}\omega_{\alpha\gamma}(r) = 1$ represents the geometry of solvent molecules [$\omega_{\alpha\gamma}(r) = 0$ for sites $\alpha$ and $\gamma$ on different solvent species] and, for relatively stiff solvent molecules, is adequately represented with rigid bonds of length $l_{\alpha\gamma}$ as $\omega_{\alpha\gamma}(r) = \delta(r - l_{\alpha\gamma})/(4\pi l_{\alpha\gamma}{}^2)$ and specified in the reciprocal $k$ space as $\omega_{\alpha\gamma}(k) = j_0(kl_{\alpha\gamma})$ in terms of the zero-order spherical function $j_0(x)$. In advance to the 3D-RISM−KH calculation, the radial total correlation function $h_{\alpha\gamma}(\mathbf{r})$ between sites $\alpha$ and $\gamma$ enumerating all sites on all sorts of molecules in the bulk solvent is obtained from the dielectrically consistent RISM (DRISM) theory[80,81] coupled with the KH closure (DRISM−KH theory),[43,48] which is applied to the liquid and supercritical $CO_2$ solvents.

The solvation free energy $\mu_\mathrm{solv}^\mathrm{KH}$ of a solute in liquid and supercritical $CO_2$ solvents following the 3D-RISM−KH integral eqs 1 and 2 is given by the closed analytical expression[43−46]

$$\mu_\mathrm{solv}^\mathrm{KH} = k_\mathrm{B}T \sum_\gamma \rho_\gamma \int \mathrm{d}\mathbf{r}\left[\frac{1}{2}h_\gamma{}^2(\mathbf{r})\Theta(-h_\gamma(\mathbf{r})) - c_\gamma(\mathbf{r}) - \frac{1}{2}h_\gamma(\mathbf{r})c_\gamma(\mathbf{r})\right] \tag{3}$$

where the sum goes over all of the sites of all solvent species and $\Theta(x)$ is the Heaviside step function.

The potential of mean force (PMF) between the koalinite platelet and the model bitumen molecule at separation $d$ comprises the difference between their interaction energies at separation d and at a large distance d0 (set in the current calculation to configuration "90° far" (see below)) calculated using the PW91 density functional plus the difference between their solvation free energies at separation $d$ and at a large distance $d_0$ (set in the current calculation as $d_0$ = 15 Å).

$$\mathrm{PMF}(d) = E_\mathrm{PW91}(d) - E_\mathrm{PW91}(d_0) + \mu(d) - \mu(d_0) \tag{4}$$

The strength of interaction of a solvent site with the solute is calculated using eq 5 as the natural logarithm of the maximum of $g_\gamma(\mathbf{r})$

$$W_\gamma = -k_\mathrm{B}T \ln g_\gamma^\mathrm{max} \tag{5}$$

where $k_\mathrm{B}$ is the Boltzmann constant and $T$ is the temperature. More detailed descriptions of the 3D-RISM−KH molecular theory of solvation are presented elsewhere.[43−48,63]

**Computational Details for 1D/3D-RISM−KH.** The solute containing a kaolinite platelet and a molecule adsorbed on it optimized using the PW91 functional is placed in a $CO_2$ solvent box of the same size as the PBC cell, and the 3D-RISM integral eqs 1 and 2 are converged on a 3D grid of 64 × 64 × 128 points. The PMF is calculated with respect to the molecule−kaolinite distance along the $z$


DOI: 10.1021/ef502202q
Energy Fuels 2015, 29, 2853−2863

Table 1. Relative Energy Values ($E_{PW91}$, kcal/mol) and Interaction Distances ($d$, Å) Calculated for the Geometries Optimized Using the DMol$^3$/PW91/DNP Method

| | phenanthridine | | benzothiophene | | tetralin | | naphthalene | |
|---|---|---|---|---|---|---|---|---|
| initial orientation | $E_{PW91}$[a] | $d$[b] | $E_{PW91}$[a] | $d$[b] | $E_{PW91}$[a] | $d$[b] | $E_{PW91}$[a] | $d$[b] |
| 0° | 6.94 | 3.24[c] | 5.61 | 3.50[c] | 0.00[a] | 2.51[f] | 2.45 | 2.74[g] |
| 45° | 0.93 | 1.92[d] | 1.19 | 2.54[e] | 0.62 | 2.45[f] | 0.00[a] | 2.41[g] |
| 90° | 0.00[a] | 1.90[d] | 0.00[a] | 2.41[e] | 2.88 | 2.50[f] | 0.39 | 2.29[g] |
| 90° far | 10.38 | 30.00 | 4.98 | 30.00 | 5.08 | 30.00 | 5.97 | 30.00 |

[a]$E_{PW91}$ is calculated relative to the most stable conformation for each system that is selected as the origin (0.00 kcal/mol). [b]Distance between the kaolinite platelet and the molecule. See footnotes *c*−*f* for details. [c]The distance between the best fit plane of the molecule and the plane of the H of axial OH of Al−OH. [d]The shortest distance is the hydrogen bond between N(phenanthridine) and H of Al−OH. [e]The shortest distance is between the H at C6 of benzothiophene and the O atom of the equatorial OH group of Al−OH. [f]The shortest distance is between an aliphatic H atom and the plane of axial H atoms of Al−OH. [g]The shortest distance is between an aromatic H atom and the plane of axial H atoms of Al−OH.

axis. The three-site model of $CO_2$ solvent built to account for quadrupole interactions that are important to correctly describe the increased orientational correlations and ordering in the fluid state is used.[82,83] This $CO_2$ solvent model has been extensively validated by Koga et al. for the solvation of naphthalene in supercritical $CO_2$.[84] The density and dielectric constant of liquid and supercritical $CO_2$ are taken from the transformer ratio-arm bridge with three-terminal capacitance cell measurements by Moriyoshi et al.[28] and listed in Table S1 of the Supporting Information. The united atom optimized potentials for liquid simulations (OPLS) force field is used for ethane solvent.[85] The density and dielectric constant values for ethane are taken from the study by Younglove and Ely[86] and listed in Table S2 of the Supporting Information. Nonbonding parameters and partial charges for the kaolinite atoms are adopted from the CLAYFF general force field developed by Cygan et al.[71] For the bitumen model compounds, we use the nonbonded parameters $\sigma$ and $\varepsilon$ from the OPLS all-atom force field[87,88] and atomic charges calculated using the MOPAC2012 computational chemistry software,[89] as in our previous studies.[68,69]

## ■ RESULTS AND DISCUSSION

**DFT in PBC Calculations.** The PW91/DNP method implemented in the DMol$^3$ software was used to fully optimize the geometries of the bitumen model compounds on kaolinite. The adsorption on the silicon oxide surface of kaolinite is weaker than that on the aluminum hydroxide surface. The values of the total energy $E_{PW91}$ of the fully optimized structures of each molecule adsorbed on the aluminum hydroxide surface obtained from the three initial orientations are listed in Table 1, relative to the global minimum defined as the lowest energy optimized structure with energy set to zero. The global minima for phenanthridine, benzothiophene, tetralin, and naphthalene on kaolinite are calculated from initial orientations of 90°, 90°, 0°, and 45°, respectively. For the optimized lowest energy structure of each molecule on kaolinite, the second Hessian matrix was calculated to confirm the absence of imaginary frequencies and ensure that the optimized structures correspond to minima of the potential energy surface. The initial orientation of "90° far" corresponds to a fully separated (non-interacting) molecule and kaolinite, and its $E_{PW91}$ value in Table 1 taken with a negative sign gives the global adsorption energy of the molecule. The adsorption strength decreases in the order phenanthridine ($E_{PW91}$ = 10.8 kcal/mol) > naphthalene ($E_{PW91}$ = 5.97 kcal/mol) > tetralin ($E_{PW91}$ = 5.08 kcal/mol) ∼ benzothiophene ($E_{PW91}$ = 4.98 kcal/mol).

The adsorption of phenanthridine on kaolinite is the strongest, because of the hydrogen bond between the N atom of phenanthridine and the H atom from the axial hydroxyl group of the kaolinite platelet N···H(axial Al−OH). The optimized hydrogen bond length of 1.90 Å (Table 1) compares favorably to the 1.8 Å reported by Johnson and Otero-dela-Roza[38] for the N···H(axial Al−OH) pyridine−kaolinite hydrogen bond that is less hindered sterically than the phenanthridine-kaolinite hydrogen bond. Also, 1.90 Å is within the 1.8−2.0 Å range predicted on the basis of the 3D-RISM−KH method for the adsorption of phenanthridine on kaolinite in toluene solvent at room temperature.[69]

Because of the rather small positive charge, the S atom of benzothiophene does not participate in specific interactions with the surface hydroxyl groups of kaolinite. The perpendicular configuration of benzothiophene is stabilized by a hydrogen bond between the H atom at $C_6$ and the equatorial OH group of kaolinite H(Ar)···O(equatorial Al−OH) with a length of 2.41 Å. The optimized geometry of naphthalene is stabilized by electrostatic interactions between $\alpha$H atoms and the O atoms of the equatorial hydroxyl groups of kaolinite ($d_{\alpha H-O}$ = 2.62 Å) as well as by van der Waals interactions. The angle between the aromatic plane of naphthalene and the plane of the surface H atoms of kaolinite is 39°, while the 90° configuration is less stable by 0.39 kcal/mol. This tilted configuration accommodates weak hydrogen-bonding interactions H(Ar)···O(equatorial Al−OH) between aromatic H atoms and the O atoms of the equatorial hydroxyl groups of kaolinite as well as OH−$\pi$ interactions involving kaolinite surface dipole and aromatic $\pi$ systems, similar to benzene adsorbed on kaolinite.[38] The hydrocarbon tetralin contains aliphatic and aromatic rings fused together and adsorbs the strongest in its planar configuration. The angle between tetralin and the kaolinite H atoms is 22° to accommodate not only hydrogen-bonding interactions of the H atoms of the aromatic ring but also van der Waals CH−O interactions of aliphatic H atoms with surface dipoles of kaolinite hydroxyl groups, similar to hexane adsorbed on kaolinite.[38] Such dispersion interactions involving induced dipoles also determine the aggregation of tetralin and other hydrocarbons containing fused aliphatic and aromatic rings.[90]

In Figure 1, we present the optimized geometries of the adsorbates on kaolinite. The hydrogen bond between the N atom of phenanthridine and the H atom of the axial OH group of kaolinite is marked with a dashed line. The heterocycles adsorb preferentially in configuration perpendicular to the kaolinite surface. These results are in agreement with the experimental and computational studies of the adsorption affinity and capacity of phenanthridine and benzothiophene on kaolinite based on the 3D-RISM−KH molecular theory of solvation.[69] Naphthalene and tetralin adsorb at 39° and 22° angles, respectively, relative to the plane of the axial H atoms of kaolinite.


DOI: 10.1021/ef502202q
Energy Fuels 2015, 29, 2853−2863

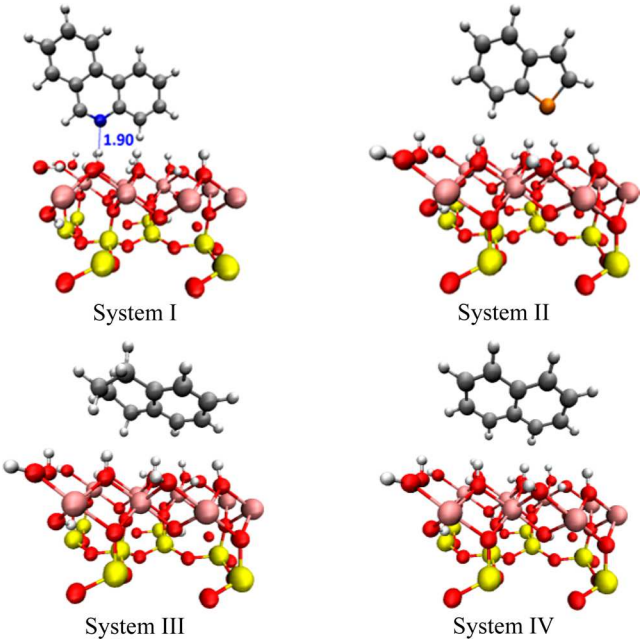


**Figure 1.** Optimized geometries for the systems containing phenanthridine (system I), benzothiophene (system II), tetralin (system III), and naphthalene adsorbed to kaolinite (system IV) in PBC using the DMol$^3$/PW91/DNP method. The N···H bond is shown as a dashed line, and its length is listed in angstroms.

**Solvation Structure of $CO_2$.** In Figure 2, we present the isosurfaces of 3D site density distribution functions $g_\gamma(\mathbf{r})$ that provide molecular insights into the mechanism of solute−$CO_2$ interactions. The preferred orientation of C and O sites of $CO_2$ deduced from the $g_\gamma(\mathbf{r})$ isosurfaces is shown using a stick $CO_2$ molecule model (see the legend in Figure 2Ia). The $g_\gamma(\mathbf{r})$ isosurfaces calculated using the 3D-RISM−KH method suggest a set of statistically probable solvent orientations that are more realistic for a solvent at room temperature than, for example, an optimized solvent geometry.[64]

At the kaolinite surface, we note two predominant orientations of $CO_2$, at axial and equatorial hydroxyl groups because of the exposure of the hydroxyl group H and O atoms, respectively, to the solvent. At axial hydroxyl groups, the O site isosurface (in purple color) is shown above the H atom, indicating hydrogen bonding, as pointed out with the arrow and call box in the top right of Figure 2Ia. The C site isosurface (in cyan color) is shown above the O site isosurface, and the preferred axial orientation of $CO_2$ is visualized using a $CO_2$ molecule perpendicular to the kaolinite surface in the top right corner. At equatorial hydroxyl groups, it is the C site of $CO_2$ that interacts with the O atom of Al−OH, in a Lewis acid−base interaction mode, and the preferred orientation of $CO_2$ is parallel to the kaolinite plane, as pointed out with the call boxes in the top and bottom left. The hydrogen bond between the N atom of phenanthridine and the axial hydroxyl group of kaolinite is shown as a dashed blue line, as pointed out in the left call box. The preferred orientations of $CO_2$ perpendicular and parallel to the kaolinite plane are also shown in the top

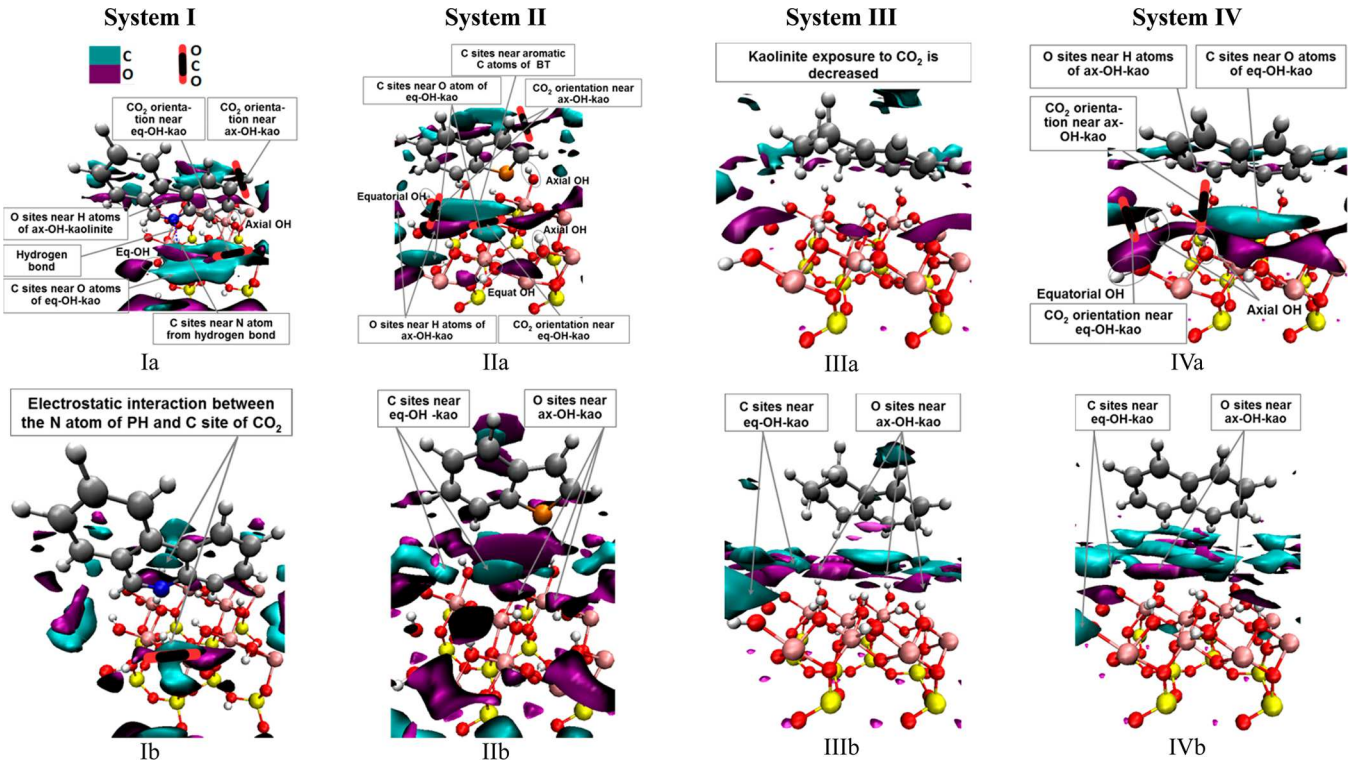


**Figure 2.** Isosurfaces of the 3D site density distribution functions $g_\gamma(r)$ of $CO_2$ for (system I) phenanthridine, (system II) benzothiophene, (system III) tetralin, and (system IV) naphthalene adsorbed on kaolinite at adsorption distances of (Ia) 2.25 Å, (IIa) 2.00 Å, (IIIa) 2.00 Å, and (IVa) 2.00 Å as well as desorption barrier distances of (Ib) 3.75 Å, (IIb) 4.50 Å, (IIIb) 3.75 Å, and (IVb) 3.75 Å. Isosurface colors: C, cyan; O, purple [$g$(C) = 3.0, and $g$(O) = 3.0]. Solute atom colors: O, red; H, white; Al, pink; Si, yellow; C, gray; N, dark blue; and S, orange. Major interactions are highlighted with arrows and described. ax-OH-kao, axial OH on the kaolinite surface; eq-OH-kao, equatorial OH on the kaolinite surface; PH, phenanthridine; and BT, benzothiophene.



DOI: 10.1021/ef502202q
Energy Fuels 2015, 29, 2853−2863

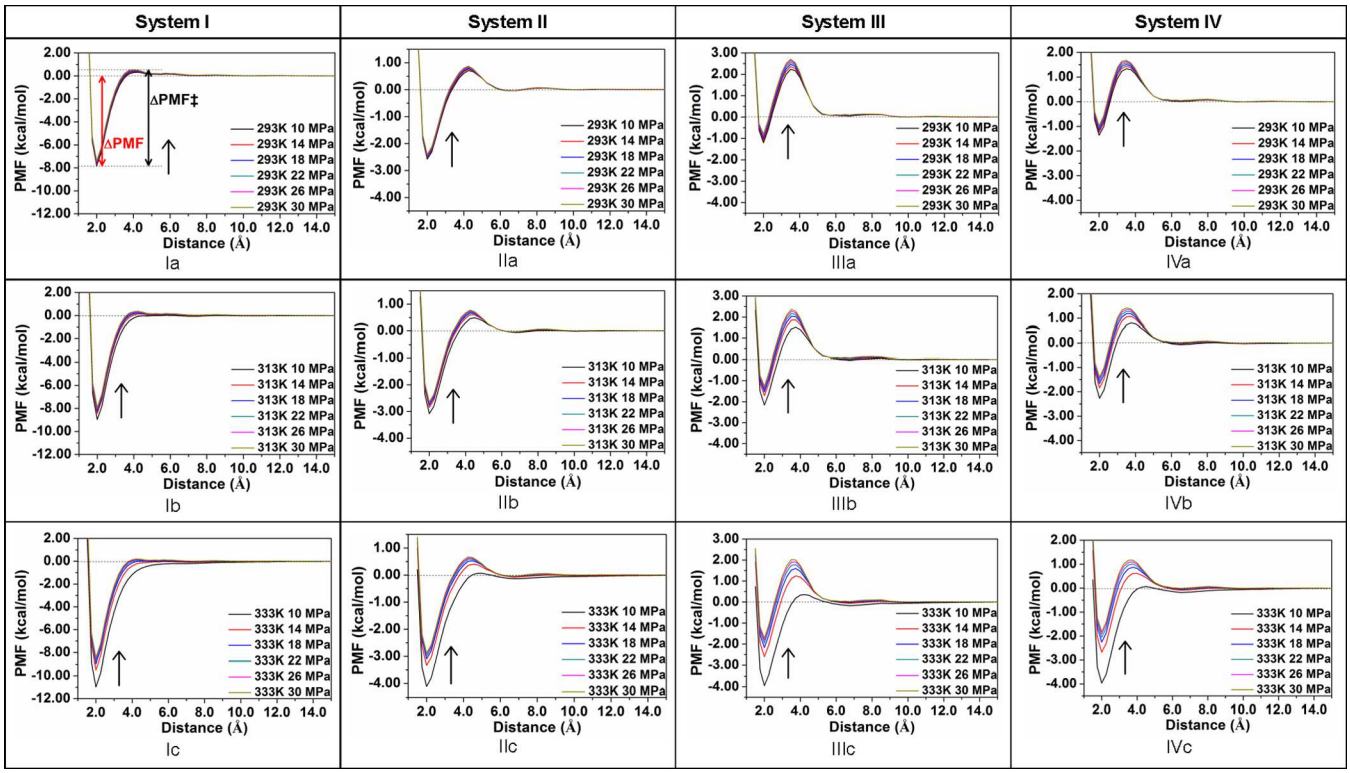


**Figure 3.** Potential of mean force (PMF) for adsorption of (system I) phenanthridine, (system II) benzothiophene, (system III) tetralin, and (system IV) naphthalene on kaolinite in a $CO_2$ solvent at temperatures of (a) 293.13 K, (b) 313.13, and (c) 333.13 K and pressures of 10−30 MPa. Arrows show the PMF increase as the pressure is increased.

right and bottom left, respectively, for the benzothiophene system in Figure 2IIa. Because the adsorption configuration of benzothiophene on kaolinite is similar to that of phenanthridine, the $CO_2$ orientation in IIb is also rather similar. The adsorption configuration of tetralin precludes a more extensive contact surface and less exposure to the $CO_2$ solvent. Because of the 39° adsorption angle, naphthalene has an intermediate contact surface and more extensive exposure of kaolinite to $CO_2$. The solvent orientations are similar to those in panels Ia and IIa of Figure 2.

The interaction of $CO_2$ with the adsorbate molecules would be notable if the molecules are desorbed from the kaolinite surface at a distance corresponding to the desorption barrier, as shown in panels Ib−IVb of Figure 2. Electrostatic (and Lewis acid−base type) interactions cause the C site of $CO_2$ to become localized near the N atom of phenanthridine and the $CO_2$ molecules to be oriented parallel to the kaolinite surface, as pointed out in Figure 2Ib. The orientation of $CO_2$ is mainly determined by the strongly charged sites of kaolinite, and the influence of the molecules is rather small.

**PMF in Liquid and Supercritical $CO_2$.** The 3D-RISM-KH molecular theory of solvation was employed to calculate the solvation free energy $\mu_{solv}^{KH}$ (eq 3) and PMF (eq 4) for desorption of phenanthridine, benzothiophene, naphthalene, and tetralin from kaolinite in a $CO_2$ solvent at temperatures of 293.15, 313.15, and 333.15 K and pressures of 10.0, 14.0, 18.0, 22.0, 26.0, and 30.0 MPa (see Table S1 of the Supporting Information for input parameters). Carbon dioxide is liquid at 293.15 K and 10−30 MPa and supercritical in the rest of the conditions studied.

In Figure 3, we present the PMF calculated for systems I−IV in liquid and supercritical $CO_2$. The distance ($x$ axis) is defined between the atom in the molecule that has the smallest $z$ coordinate and the plane of the H atoms at the aluminum hydroxide surface of kaolinite. Important features of the PMF are defined in Figure 3Ia. The PMF minimum ΔPMF corresponds to the solvated geometry of the organic molecule adsorbed on the kaolinite surface and is referred to as adsorption free energy. The barrier for desorption, $\Delta PMF^{\ddagger}$, of an organic molecule from kaolinite is defined as the difference between the maximum and minimum of the PMF. The local PMF minima at ∼6.0 Å that are best noted in Figure 3IIIa correspond to the free energy for the formation of the first solvation shell and represent a fully solvated organic molecule and kaolinite platelet. These minima are not well-defined for the other systems because of small contact surfaces.

The PMF plots (Figure 3) show that ΔPMF increases as the pressure is increased, as shown with black arrows pointing up. The effect of the pressure on the PMF is rather weak in liquid $CO_2$ at 293 K and becomes very well pronounced in supercritical $CO_2$ as the temperature is increased to 313 K and even 333 K. The barrier for disaggregation, relevant to the kinetics of disaggregation, is well-pronounced for systems II−IV and increases as the pressure is increased and the temperature is decreased, conditions corresponding to increasing solvent density. For system I at 313 and 333 K, this barrier is the same as the adsorption free energy ΔPMF.

The desorption barriers $\Delta PMF^{\ddagger}$ of the bitumen model compounds listed in Table 2 increase as the pressure is decreased and the temperature is increased. The adsorption barriers ($\Delta PMF^{\ddagger} - |\Delta PMF|$) increase as the pressure is increased and the temperature is decreased, which is opposite the $\Delta PMF^{\ddagger}$ trend. The effect of the $CO_2$ temperature and pressure on these kinetic barriers is very small (∼0.2−0.3 kcal/


DOI: 10.1021/ef502202q
Energy Fuels 2015, 29, 2853−2863

**Table 2. Barrier for Desorption ΔPMF‡ of (System I) Phenanthridine, (System II) Benzothiophene, (System III) Tetralin, and (System IV) Naphthalene on Kaolinite in kcal/mol**

| | 10 MPa | 14 MPa | 18 MPa | 22 MPa | 26 MPa | 30 MPa |
|---|---|---|---|---|---|---|
| | | | ΔPMF‡ for System I | | | |
| 293 K | 8.15 | 8.07 | 8.01 | 7.96 | 7.93 | 7.89 |
| 313 K | 8.92 | 8.58 | 8.46 | 8.38 | 8.32 | 8.27 |
| 333 K | 10.15 | 9.26 | 8.95 | 8.80 | 8.70 | 8.65 |
| | | | ΔPMF‡ for System II | | | |
| 293 K | 3.28 | 3.26 | 3.28 | 3.26 | 3.28 | 3.28 |
| 313 K | 3.54 | 3.45 | 3.43 | 3.42 | 3.42 | 3.42 |
| 333 K | 4.01 | 3.69 | 3.60 | 3.57 | 3.55 | 3.55 |
| | | | ΔPMF‡ for System III | | | |
| 293 K | 3.44 | 3.46 | 3.47 | 3.48 | 3.50 | 3.51 |
| 313 K | 3.60 | 3.58 | 3.59 | 3.60 | 3.61 | 3.62 |
| 333 K | 3.85 | 3.72 | 3.70 | 3.70 | 3.72 | 3.74 |
| | | | ΔPMF‡ for System IV | | | |
| 293 K | 2.70 | 2.68 | 2.67 | 2.66 | 2.65 | 2.65 |
| 313 K | 3.00 | 2.89 | 2.85 | 2.84 | 2.83 | 2.82 |
| 333 K | 3.50 | 3.16 | 3.06 | 3.02 | 2.99 | 2.98 |

mol) in liquid $CO_2$ and increases to 0.5−1.5 kcal/mol in supercritical conditions, suggesting that effective desorption rate control can be accomplished in the latter conditions.

In Figure 4, we present 3D plots correlating the adsorption free energy ΔPMF with the temperature and pressure that show the extraction of bitumen model compounds from kaolinite is most favored at 293 K and 30 MPa, whereas extraction at 333 K and 10 MPA requires the most energy. These results indicate that the adsorption free energies in $CO_2$ decrease in the order phenanthridine > benzthiophene > naphthalene > tetralin, which differs from that in the gas phase (Table 1). The $CO_2$ solvent facilitates desorption of tetralin and naphthalene by most effectively solvating naphthenic hydrocarbons followed by aromatic hydrocarbons, while heterocycles are very weakly stabilized by solvation. The adsorption energies of tetralin and naphthalene range from −0.80 to −3.95 kcal/mol and from −0.97 to −3.97 kcal/mol, respectively, indicating that these two components would be very difficult to separate using a $CO_2$ solvent. The results also indicate that the hydrocarbon adsorption energies are less than 1 kcal/mol at 293 K and 30 MPa in liquid $CO_2$ (the thermodynamic state with the highest density of $CO_2$), which implies that uptake by liquid $CO_2$ would be favored. The adsorption energy of benzothiophene ranges from −2.40 to −4.11 kcal/mol, which is substantially smaller than that of the rest and indicates that this compound is the least sensitive to the temperature and pressure effects of $CO_2$. Benzothiophene can be separated from the hydrocarbons at the low-temperature and high-pressure conditions studied. The adsorption energy of phenanthridine ranges from −7.38 to −10.98 kcal/mol, which is the largest variation and indicates that this compound is the most sensitive to the temperature and pressure effects of $CO_2$. Even at high pressure in liquid $CO_2$, phenanthridine would be

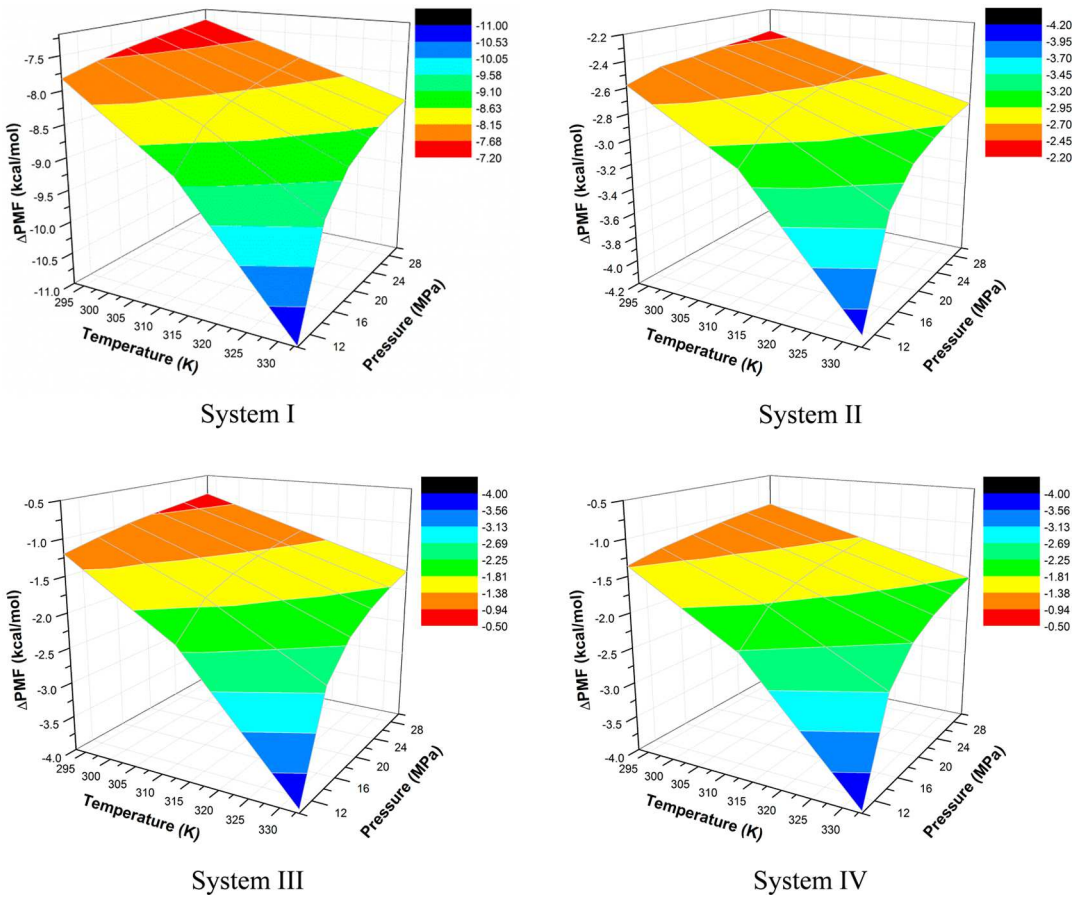


**Figure 4.** Adsorption free energies (ΔPMF) versus the temperature and pressure for (system I) phenanthridine−kaolinite, (system II) benzothiophene−kaolinite, (system III) tetralin−kaolinite, and (system IV) naphthalene−kaolinite systems in liquid and supercritical $CO_2$ solvents.


DOI: 10.1021/ef502202q
Energy Fuels 2015, 29, 2853−2863

adsorbed on kaolinite because of the stronger hydrogen bonding to the hydroxyl group compared to the electrostatic N−C($CO_2$) interaction. At a low temperature and high pressure in liquid $CO_2$, the heterocycles would remain adsorbed on kaolinite, suggesting an approach for the effective extraction of deasphalted bitumen.

These results correlate with experimental findings in showing that the recovery of hydrocarbons increases as the pressure is increased and the temperature is decreased.[30−32] The destiny of heterocyclic compounds during extraction has not been thoroughly investigated in the literature. Asphaltene precipitation studies have shown that the functional groups present in the precipitate in supercritical $CO_2$ are similar to those precipitated out of paraffinic solvents based on the standard saturates, aromatics, resins, and asphaltenes (SARA) analysis,[33] without further S and N content analysis.

For comparison, we calculate the adsorption energies ΔPMF for systems I−IV in liquid ethane solvent at the temperature of 293 K and pressures of 10 and 18 MPa as well as in critical ethane solvent at the temperature of 333 K and pressures of 10 and 18 MPa. It is important to note that the change in both density and dielectric constant of ethane is smaller than that of the $CO_2$ solvent in these conditions, as listed in Tables S1 and S2 of the Supporting Information. The results show that ΔPMF is less sensitive to temperature and pressure changes in ethane compared to the $CO_2$ solvent, suggesting that the latter solvent allows for better control of the desorption of these organic molecules from kaolinite as well as more favorable conditions for selective desorption or deasphalting (see Table S3 of the Supporting Information).

In Table 3, we list the strength of the interaction of $CO_2$ solvent sites with solute systems I−IV calculated using eq 5. The strongest interactions are of the C and O sites of $CO_2$ with O and H atoms, respectively, of equatorial and axial hydroxyl groups on the aluminum hydroxide surface of kaolinite. The interaction of the C site is stronger because of its twice larger charge compared to an O site, despite the O sites being more sterically accessible. The results indicate that the interaction of $CO_2$ with the kaolinite platelet is stronger than that with the molecule, because of the larger (by absolute value) atomic charges in kaolinite. For the organic molecules, the strongest interactions are of C sites of $CO_2$, with the aromatic C atoms delocalized above and below the centers of the phenyl rings and with the N atom of phenanthridine. The interactions of C sites of $CO_2$ with the aluminum hydroxide surface of kaolinite are stronger than those of toluene solvent sites (0.6−0.8 kcal/mol).[69]

**Table 3. Strength of Interaction $W_\gamma$ of the Solvent Sites of $CO_2$ with the Solute Systems (I) Phenanthridine−Kaolinite, (II) Benzothiophene−Kaolinite, (III) Benzothiophene−Tetralin, and (IV) Benzothiophene−Naphthalene in the Optimized Geometry (at the PMF Minimum)[a]**

| system | solvent site | localization | $g_\gamma^{max}$ | $W_\gamma$ |
|---|---|---|---|---|
| I | C | O of Al−OH | 5.80 | −1.04 |
| | | N of Ph | 2.80 | −0.61 |
| | O | H of Al−OH | 3.60 | −0.76 |
| | | O of Ph | 2.80 | −0.61 |
| II | C | O of Al−OH | 4.30 | −0.86 |
| | | C of BT | 3.60 | −0.76 |
| | O | H of Al−OH | 3.90 | −0.81 |
| | | C of BT | 2.80 | −0.61 |
| III | C | O of Al−OH | 4.30 | −0.86 |
| | | C of TR | 3.80 | −0.79 |
| | O | H of Al−OH | 3.80 | −0.79 |
| | | C of TR | 3.00 | −0.65 |
| IV | C | O of Al−OH | 4.10 | −0.84 |
| | | C of NT | 2.90 | −0.63 |
| | O | H of Al−OH | 3.90 | −0.81 |
| | | C of NT | 2.80 | −0.61 |

[a]In localization, H and O are solute atoms at the aluminum hydroxide (Al−OH) surface of kaolinite, N of Ph is the N atom of phenanthridine, C of Ph is the benzyl aromatic C atom of phenanthridine, C of BT is the αC atom of benzothiophene, C of TR is the aromatic C atom of tetralin, and C of NT is the C atom of naphthalene.

## ■ CONCLUSION

The geometries of systems containing the bitumen model compounds phenanthridine, benzothiophene, tetralin, and naphthalene adsorbed on a kaolinite platelet are optimized in PBC and gas phase using the PW91/DNP method. The strongest adsorption is calculated for phenanthridine because of N···H(axial Al−OH) hydrogen bonding, followed by naphthalene because of H(Ar)···O(equatorial Al−OH) hydrogen bonding, and tetralin and benzothiophene because of van der Waals and weaker H(Ar)···O(equatorial Al−OH) interactions.

To study the effect of the $CO_2$ solvent, the PMF between kaolinite and bitumen model compounds is calculated using the 3D-RISM−KH molecular theory of solvation at temperatures of 293−333 K and pressures of 10−30 MPa. The results show strong electrostatic interactions of the C site of $CO_2$ with the O atoms of equatorial hydroxyl groups, followed by hydrogen-bonding interactions of the O site of $CO_2$ with H atoms of axial hydroxyl groups of kaolinite, and electrostatic interactions of the C site of $CO_2$ with the N atom of phenanthridine. The interactions of thiophene and aromatic and aliphatic moieties with $CO_2$ are delocalized and hydrophobic.

The PMF results indicate that the adsorption of hydrocarbons on kaolinite is rather weak in liquid $CO_2$, suggesting that these would be desorbed preferentially, while the heterocycles remain adsorbed. Phenanthridine and benzothiophene are found to be the most and least sensitive, respectively, to $CO_2$ temperature and pressure changes. The kinetic barrier for disaggregation is the most sensitive to the temperature and pressure of $CO_2$ in supercritical conditions, highlighting the importance of further studies in this area. These results provide important insight into the mechanism of adsorption and solvation of kaolinite and bitumen components and are aimed to help develop approaches to use liquid and supercritical $CO_2$ for extraction of bitumen from oil sands.

Experimental desorption studies conducted using pure compounds are necessary for understanding the mechanism of solvation of heavy oil components in a $CO_2$ solvent. Collaborative experimental and computational studies could help optimize the external conditions for extraction of heavy oils from different sources based on mechanistic insight. Moreover, understanding the mechanism of action of additives (also called co-solvents), such as heavy hydrocarbons, alcohols,[91] and salty water,[30] could help improve the efficiency of the $CO_2$-based extraction processes. Solvent systems containing $CO_2$ present important alternatives to organics and could be valuable for the development of improved non-aqueous extraction processes.


DOI: 10.1021/ef502202q
Energy Fuels 2015, 29, 2853−2863

## ■ ASSOCIATED CONTENT

### Supporting Information

Physical parameters of dense $CO_2$ and ethane solvents and additional results. This material is available free of charge via the Internet at http://pubs.acs.org.

## ■ AUTHOR INFORMATION


### Corresponding Authors

*E-mail: stoyanov@ualberta.ca.
*E-mail: walk@vm.uff.br.
*E-mail: tadek.dabros@nrcan-rncan.gc.ca.
*E-mail: andriy.kovalenko@nrc-cnrc.gc.ca.


### Notes

The authors declare no competing financial interest.

## ■ ACKNOWLEDGMENTS

This work is supported by the National Institute for Nanotechnology (NINT), a joint initiative of the National Research Council of Canada, the University of Alberta, the Government of Alberta, and the Government of Canada. Stanislav R. Stoyanov and Andriy Kovalenko acknowledge the financial support of the Imperial Oil–Alberta Innovates Energy and Environment Solutions Institute for Oil Sands Innovation (IOSI) at the University of Alberta. Mateus Ribeiro Lage and José Walkimar de Mesquita Carneiro are grateful to the Brazilian agency Coordenação de Aperfeiçoamento de Pessoal de Nível Superior (CAPES) for Ph.D. and research fellowships, respectively. The agency Fundação Carlos Chagas Filho de Amparo à Pesquisa do Estado do Rio de Janeiro (FAPERJ) also supported the work at the Fluminense Federal University. Stanislav R. Stoyanov thanks Dr. John M. Villegas for discussion. The computations were performed on the high-performance computing resources provided by WestGrid and Compute/Calcul Canada as well as at the Integrated Nanosystems Research Facility (INRF) at the University of Alberta.

## ■ REFERENCES


(1) International Energy Agency (IEA). *World Energy Outlook 2010*; IEA: Paris, France, 2010.

(2) Butler, R. M.; McNab, G. S.; Lo, H. Y. Theoretical studies on the gravity drainage of heavy oil during in-situ steam heating. *Can. J. Chem. Eng.* **1981**, *59*, 455–460.

(3) Masliyah, L.; Zhou, Z.; Xu, Z.; Czarnecki, J.; Hamza, H. Understanding water-based bitumen extraction from Athabasca oil sands. *Can. J. Chem. Eng.* **2004**, *82*, 628–654.

(4) Das, S. K. Vapex: An efficient process for the recovery of heavy oil and bitumen. *SPE J.* **1998**, *3*, 232–237.

(5) Brough, S. A.; Riley, S. H.; McGrady, G. S.; Tanhawiriyakul, S.; Romero-Zerón, L.; Willson, C. D. Low temperature extraction and upgrading of oil sands and bitumen in supercritical fluid mixtures. *Chem. Commun.* **2010**, *46*, 4923–4925.

(6) Painter, P.; Williams, P.; Mannebach, E. The recovery of bitumen from oil or tar sands using ionic liquids. *Energy Fuels* **2010**, *24*, 1094–1098.

(7) Hooshiar, A.; Uhlik, P.; Ivey, D. G.; Liu, Q.; Etsell, T. H. Clay minerals in nonaqueous extraction of bitumen from Alberta oil sands. Part 2. Characterization of clay minerals. *Fuel Process. Technol.* **2012**, *96*, 183–194.

(8) Wu, J.; Dabros, T. Process for solvent extraction of bitumen from oil sand. *Energy Fuels* **2012**, *26*, 1002–1008.

(9) Long, Y.; Dabros, T.; Hamza, H. Selective solvent deasphalting for heavy oil emulsion treatment. In *Asphaltenes, Heavy Oils, and Petroleomics*; Mullins, O. C., Sheu, E. Y., Hammami, A., Marshall, A. G., Eds.; Springer Science and Business Media: New York, 2007; pp 511–547.

(10) Harjai, S. K.; Flury, C.; Masliyah, J.; Drelich, J.; Xu, Z. Robust aqueous–nonaqueous hybrid process for bitumen extraction from mineable Athabasca oil sands. *Energy Fuels* **2012**, *26*, 2920–2927.

(11) Yang, Z.; Li, Q.; Hua, R.; Gray, M. R.; Chou, K. C. Competitive adsorption of toluene and *n*-alkanes at binary solution/silica interfaces. *J. Phys. Chem. C* **2009**, *113*, 20355–20359.

(12) Buckingham, A. D.; Disch, R. L. The quadrupole moment of the carbon dioxide molecule. *Proc. R. Soc. London, Ser. A* **1963**, *273*, 275–289.

(13) Li, J.-R.; Kuppler, R. J.; Zhou, H.-C. Selective gas adsorption and separation in metal–organic frameworks. *Chem. Soc. Rev.* **2009**, *38*, 1477–1504.

(14) Bae, Y.-S.; Lee, C.-H. Sorption kinetics of eight gases on a carbon molecular sieve at elevated pressure. *Carbon* **2005**, *43*, 95–107.

(15) Beckman, E. J. Supercritical and near-critical $CO_2$ in green chemical synthesis and processing. *J. Supercrit. Fluids* **2004**, *28*, 121–191.

(16) Kim, K. H.; Kim, Y. Theoretical studies for the supercritical $CO_2$ solubility of organophosphorous molecules: Lewis acid–base interactions and C–H···O weak hydrogen bonding. *Bull. Korean Chem. Soc.* **2007**, *28*, 2454–2458.

(17) Raveendran, P.; Wallen, S. L. Cooperative C–H···O hydrogen bonding in $CO_2$–Lewis base complexes: Implications for solvation in supercritical $CO_2$. *J. Am. Chem. Soc.* **2002**, *124*, 12590–12599.

(18) Bell, P. W.; Thote, A. J.; Park, Y.; Gupta, R. B.; Roberts, C. B. Strong Lewis acid–Lewis base interactions between supercritical carbon dioxide and carboxylic acids: Effects on self-association. *Ind. Eng. Chem. Res.* **2003**, *42*, 6280–6289.

(19) Kilic, S.; Michalik, S.; Wang, Y.; Johnson, J. K.; Enick, R. M.; Beckman, E. J. Effect of grafted Lewis base groups on the phase behavior of model poly(dimethyl siloxanes) in $CO_2$. *Ind. Eng. Chem. Res.* **2003**, *42*, 6415–6424.

(20) Lake, L. W. *Enhanced Oil Recovery*; Prentice Hall: Englewood Cliffs, NJ, 1989.

(21) Chakma, A.; Islam, M. R. *Enhanced Oil Recovery (AIChE Symposium Series)*; Berruti, F., Eds.; American Institute of Chemical Engineers: New York, 1991; Vol. *280*.

(22) Macedo, J. C. D.; Duarte, M. A. I. Catalytic cracking of heavy vacuum gas oil over aluminum diacetate containing catalyst. *Appl. Catal., A* **1994**, *110*, 87–98.

(23) Roussel, J.-C., Boulet, R. Characterization of crude oils and petroleum fractions. In *Petroleum Refining: Crude Oil, Petroleum Products, Process Flowsheets*; Wauquier, J.-P., Ed.; Editions Technip: Paris, France, 1995, Vol. *1*, pp 39–84, 453–469.

(24) Pearson, C. D.; Green, J. B. Vanadium and nickel complexes in petroleum resid acid, base, and neutral fractions. *Energy Fuels* **1993**, *7*, 338–346.

(25) Mitchell, P. C. H. Hydrodemetallisation of crude petroleum: Fundamental studies. *Catal. Today* **1990**, *7*, 439–445.

(26) McHugh, M. A.; Krukonis, V. J. *Supercritical Fluid Extraction*, 2nd ed.; Butterworth-Heinemann: Boston, MA, 1994.

(27) *Supercritical Carbon Dioxide: In Polymer Reaction Engineering*; Kemmere, M. F., Meyer, T., Eds.; Wiley-VCH Verlag GmbH & Co. KGaA: Weinhein, Germany, 2005; pp 3–35.

(28) Moriyoshi, T.; Kita, T.; Uosaki, Y. Static relative permittivity of carbon dioxide and nitrous oxide up to 30 MPa. *Ber. Bunsen-Ges..* **1993**, *97*, 589–596.

(29) Gupta, R. B.; Shim, J.-J. *Solubility in Supercritical Carbon Dioxide*; CRC Press (Taylor & Francis Group): Boca Raton, FL, 2007.

(30) Rudyk, S.; Spirov, P. Three-dimensional scheme of supercritical carbon dioxide extraction of heavy hydrocarbon mixture in (pressure; temperature; recovery) coordinates. *Energy Fuels* **2013**, *27*, 5996–6001.

(31) Rudyk, S.; Spirov, P. Upgrading and extraction of bitumen from Nigerian tar sand by supercritical carbon dioxide. *Appl. Energy* **2014**, *113*, 1397–1404.

(32) Al-Marzouqi, A. H.; Zekri, A. Y.; Jobe, B.; Dowaidar, A. Supercritical fluid extraction for the determination of optimum oil recovery conditions. *J. Petr. Sci. Eng.* **2007**, *55*, 37–47.




DOI: 10.1021/ef502202q
*Energy Fuels* 2015, 29, 2853–2863

(33) Deo, M.; Parra, M. Characterization of carbon-dioxide-induced asphaltene precipitation. *Energy Fuels* **2012**, *26*, 2672−2679.
(34) Orestes, E.; Ronconi, C. M.; Carneiro, W. M. Insights into the interactions of $CO_2$ with amines: A DFT benchmark study. *Phys. Chem. Chem. Phys.* **2014**, *16*, 17213−17219.
(35) Iida, K.; Sato, H. Proton transfer step in the carbon dioxide capture by monoethanol amine: A theoretical study at the molecular level. *J. Phys. Chem. B* **2012**, *116*, 2244−2248.
(36) Muñoz-Losa, A.; Martins-Costa, M. T. C.; Ingrosso, F.; Ruiz-López, M. F. Correlated *ab initio* molecular dynamics simulations of the acetone−carbon dioxide complex: Implications for solubility in supercritical $CO_2$. *Mol. Simul.* **2014**, *40*, 157−159.
(37) Schaef, H. T.; Glezakou, V.-A.; Owen, A. T.; Ramprasad, S.; Martin, P. F.; McGrail, B. P. Surface condensation of $CO_2$ onto kaolinite. *Environ. Sci. Technol. Lett.* **2014**, *1*, 142−145.
(38) Johnson, E. R.; Otero-de-la-Roza, A. Adsorption of organic molecules on kaolinite from the exchange-hole dipole moment dispersion model. *J. Chem. Theory Comput.* **2012**, *8*, 5124−5131.
(39) Headen, T. F.; Boek, E. S. Molecular dynamics simulations of asphaltene aggregation in supercritical carbon dioxide with and without limonene. *Energy Fuels* **2011**, *25*, 503−508.
(40) Krishnan, M.; Saharay, M.; Kirkpatrick, R. J. Molecular dynamics modeling of $CO_2$ and poly(ethylene glycol) in montmorillonite: The structure of clay−polymer composites and the incorporation of $CO_2$. *J. Phys. Chem. C* **2013**, *117*, 20592−20609.
(41) Cygan, R. T.; Romanov, V. N.; Myshakin, E. M. Molecular simulation of carbon dioxide capture by montmorillonite using an accurate and flexible force field. *J. Phys. Chem. C* **2012**, *116*, 13079−13091.
(42) Tenney, C. M.; Cygan, R. T. Molecular simulation of carbon dioxide, brine, and clay mineral interactions and determination of contact angles. *Environ. Sci. Technol.* **2014**, *48*, 2035−2042.
(43) Kovalenko, A. Three-dimensional RISM theory for molecular liquids and solid-liquid interfaces. In *Molecular Theory of Solvation*; Hirata, F., Ed.; Kluwer Academic Publishers, Dordrecht, Netherlands, 2003; Series: Understanding Chemical Reactivity, Vol. *24*, pp 169−275.
(44) Kovalenko, A.; Hirata, F. Self-consistent description of a metal−water interface by the Kohn−Sham density functional theory and the three-dimensional reference interaction site model. *J. Chem. Phys.* **1999**, *110*, 10095−10112.
(45) Kovalenko, A.; Hirata, F. Potentials of mean force of simple ions in ambient aqueous solution. I: Three-dimensional reference interaction site model approach. *J. Chem. Phys.* **2000**, *112*, 10391−10402.
(46) Kovalenko, A.; Hirata, F. Potentials of mean force of simple ions in ambient aqueous solution. II. Solvation structure from the three-dimensional reference interaction site model approach, and comparison with simulations. *J. Chem. Phys.* **2000**, *112*, 10403−10417.
(47) Gusarov, S.; Pujari, B. S.; Kovalenko, A. Efficient treatment of solvation shells in 3D molecular theory of solvation. *J. Comput. Chem.* **2012**, *33*, 1478−1494.
(48) Kovalenko, A. Multiscale modeling of solvation in chemical and biological nanosystems and in nanoporous materials. *Pure Appl. Chem.* **2013**, *85*, 159−199.
(49) Yoshida, K.; Yamaguchi, T.; Kovalenko, A.; Hirata, F. Structure of *tert*-butyl alcohol−water mixtures studied by the RISM theory. *J. Phys. Chem. B* **2002**, *106*, 5042−5049.
(50) Kovalenko, A.; Hirata, F. First-principles realization of a van der Waals−Maxwell theory for water. *Chem. Phys. Lett.* **2001**, *349*, 496−502.
(51) Kovalenko, A.; Hirata, F. Towards a molecular theory for the van der Waals−Maxwell description of fluid phase transitions. *J. Theor. Comput. Chem.* **2002**, *1*, 381−406.
(52) Tanimura, A.; Kovalenko, A.; Hirata, F. Structure of electrolyte solutions sorbed in carbon nanospaces, studied by the replica RISM theory. *Langmuir* **2007**, *23*, 1507−1517.
(53) Kovalenko, A. Molecular description of electrosorption in a nanoporous carbon electrode. *J. Comput. Theor. Nanosci.* **2004**, *1*, 398−411.
(54) Kovalenko, A.; Hirata, F. A replica reference interaction site model theory for a polar molecular liquid sorbed in a disordered microporous material with polar chemical groups. *J. Chem. Phys.* **2001**, *115*, 8620.
(55) Malvaldi, M.; Bruzzone, S.; Chiappe, C.; Gusarov, S.; Kovalenko, A. Ab initio study of ionic liquids by KS-DFT/3D-RISM-KH theory. *J. Phys. Chem. B* **2009**, *113*, 3536−3542.
(56) Kovalenko, A.; Kobryn, A. E.; Gusarov, S.; Lyubimova, O.; Liu, X.; Blinov, N.; Yoshida, M. Molecular theory of solvation for supramolecules and soft matter structures: Application to ligand binding, ion channels, and oligomeric polyelectrolyte gelators. *Soft Matter* **2012**, *8*, 1508−1520.
(57) Liu, X.; Lyubimova, O.; Kobryn, A. E.; Gusarov, S.; Kovalenko, A. Mesoscopic study of dynamics and gelation ability of oligomeric electrolyte gelator with dissipative particle dynamics. *Proc. Comput. Sci.* **2011**, *4*, 1031−1038.
(58) Kobryn, A. E.; Kovalenko, A. Molecular theory of hydrodynamic boundary conditions in nanofluidics. *J. Chem. Phys.* **2008**, *129*, 134701.
(59) Chhabra, R.; Moralez, J. G.; Raez, J.; Yamazaki, T.; Cho, J.-Y.; Myles, A. J.; Kovalenko, A.; Fenniri, H. One-pot nucleation, growth, morphogenesis, and passivation of 1.4 nm Au nanoparticles on self-assembled rosette nanotubes. *J. Am. Chem. Soc.* **2010**, *132*, 32−33.
(60) Moralez, J. G.; Raez, J.; Yamazaki, T.; Motkuri, R. K.; Kovalenko, A.; Fenniri, H. Helical rosette nanotubes with tunable stability and hierarchy. *J. Am. Chem. Soc.* **2005**, *127*, 8307−8309.
(61) Li, Q.; Gusarov, S.; Evoy, S.; Kovalenko, A. Electronic structure, binding energy, and solvation structure of the streptavidin−biotin supramolecular complex: ONIOM and 3D-RISM study. *J. Phys. Chem. C* **2009**, *113*, 9958−9967.
(62) Yamazaki, T.; Blinov, N.; Wishart, D.; Kovalenko, A. Hydration effects on the HET-s prion and amyloid-$\beta$ fibrillous aggregates, studied with three-dimensional molecular theory of solvation. *Biophys. J.* **2008**, *95*, 4540−4548.
(63) Silveira, R. L.; Stoyanov, S. R.; Gusarov, S.; Skaf, M. S.; Kovalenko, A. Plant biomass recalcitrance: Effect of hemicellulose composition on nanoscale forces that control cell wall strength. *J. Am. Chem. Soc.* **2013**, *135*, 19048−19051.
(64) Stoyanov, S. R.; Gusarov, S.; Kovalenko, A. Multiscale modeling of the adsorption interaction between model bitumen compounds and zeolite nanoparticles in gas and liquid phase. In *Industrial Applications of Molecular Simulations*; Meunier, M., Ed.; CRC Press (Taylor & Francis Group): Boca Raton, FL, 2011; pp 203−230.
(65) Stoyanov, S. R.; Gusarov, S.; Kovalenko, A. Multiscale modelling of asphaltene disaggregation. *Mol. Simul.* **2008**, *34*, 953−960.
(66) Costa, L. M.; Hayaki, S.; Stoyanov, S. R.; Gusarov, S.; Tan, X.; Gray, M. R.; Stryker, J. M.; Tykwinski, R.; Carneiro, J. W. M.; Sato, H.; Seidl, P. R.; Kovalenko, A. 3D-RISM-KH molecular theory of solvation and density functional theory investigation of the role of water in the aggregation of model asphaltenes. *Phys. Chem. Chem. Phys.* **2012**, *14*, 3922−3934.
(67) Costa, L. M.; Stoyanov, S. R.; Gusarov, S.; Tan, X.; Gray, M. R.; Stryker, J. M.; Tykwinski, R.; Carneiro, J. W. M.; Seidl, P. R.; Kovalenko, A. Density functional theory investigation of the contributions of $\pi-\pi$ stacking and hydrogen-bonding interactions to the aggregation of model asphaltene compounds. *Energy Fuels* **2012**, *26*, 2727−2735.
(68) Fafard, J.; Lyubimova, O.; Stoyanov, S. R.; Dedzo, G. K.; Gusarov, S.; Kovalenko, A.; Detellier, C. Adsorption of indole on kaolinite in non-aqueous media: Organoclay preparation, characterization, and investigation by the 3D-RISM-KH molecular theory of solvation. *J. Phys. Chem. C* **2013**, *117*, 18556−18566.
(69) Huang, W.-J.; Dedzo, G. K.; Stoyanov, S. R.; Lyubimova, O.; Gusarov, S.; Singh, S.; Lao, H.; Kovalenko, A.; Detellier, C. Molecule-surface recognition between heterocyclic aromatic compounds and kaolinite in toluene investigated by molecular theory of solvation and


DOI: 10.1021/ef502202q
*Energy Fuels* 2015, 29, 2853−2863

thermodynamic and kinetic experiments. *J. Phys. Chem. C* **2014**, *118*, 23821−23834.
(70) Perdew, J. P.; Chevary, J. A.; Vosko, S. H.; Jackson, K. A.; Pederson, M. R.; Singh, D. J.; Fiolhais, C. Atoms, molecules, solids, and surfaces: Applications of the generalized gradient approximation for exchange and correlation. *Phys. Rev. B: Condens. Matter Mater. Phys.* **1992**, *46*, 6671−6687.
(71) Delley, B. An all-electron numerical method for solving the local density functional for polyatomic molecules. *J. Chem. Phys.* **1990**, *92*, 508−517.
(72) Accelrys, Inc. *DMol$^3$, Release 4.0*; Accelrys, Inc.: San Diego, CA, 2001.
(73) Bish, D. L. Rietveld refinement of the kaolinite structure at 1.5 K. *Clays Clay Miner.* **1993**, *41*, 738−744.
(74) Lo, C.; Trout, B. L. Density-functional theory characterization of acid sites in chabazite. *J. Catal.* **2004**, *227*, 77−89.
(75) Pascale, F.; Ugliengo, P.; Civalleri, B.; Orlando, R.; D'Arco, P.; Dovesi, R. Hydrogarnet defect in chabazite and sodalite zeolites: A periodic Hartree−Fock and B3LYP study. *J. Chem. Phys.* **2002**, *117*, 5337.
(76) Tsuzuki, S.; Luthi, H. P. Interaction energies of van der Waals and hydrogen bonded systems calculated using density functional theory: Assessing the PW91 model. *J. Chem. Phys.* **2001**, *114*, 3949.
(77) Stoyanov, S. R.; Gusarov, S.; Kuznicki, S. M.; Kovalenko, A. Theoretical modeling of zeolite nanoparticle surface acidity for heavy oil upgrading. *J. Phys. Chem. C* **2008**, *112*, 6794−6810.
(78) Chandler, D.; McCoy, J.; Singer, S. Density functional theory of nonuniform polyatomic systems. I. General formulation. *J. Chem. Phys.* **1986**, *85*, 5971−5976.
(79) Chandler, D.; McCoy, J.; Singer, S. Density functional theory of nonuniform polyatomic systems. II. Rational closures for integral equations. *J. Chem. Phys.* **1986**, *85*, 5977−5982.
(80) Perkyns, J. S.; Pettitt, B. M. Site-site theory for finite concentration saline solutions. *J. Chem. Phys.* **1992**, *97*, 7656−7666.
(81) Perkyns, J. S.; Pettitt, B. M. A dielectrically consistent interaction site theory for solvent−electrolyte mixtures. *Chem. Phys. Lett.* **1992**, *190*, 626−630.
(82) Murthy, C. S.; Singer, K.; McDonald, I. R. Interaction site models for carbon dioxide. *Mol. Phys.* **1981**, *44*, 135−143.
(83) Steele, W. A.; Posch, H. A. A simulation study of the induced infrared absorption in liquid $CO_2$. *J. Chem. Soc., Faraday Trans. 2* **1987**, *83*, 1843−1858.
(84) Koga, K.; Tanaka, H.; Zeng, X. C. RISM integral equation study of local solvation behavior of naphthalene in supercritical carbon dioxide. *J. Phys. Chem.* **1996**, *100*, 16711−16719.
(85) Jorgensen, W. L.; Tirado-Rives, J. The OPLS potential functions for proteins. Energy minimizations for crystals of cyclic peptides and crambin. *J. Am. Chem. Soc.* **1988**, *110*, 1657−1666.
(86) Younglove, B. A.; Ely, J. F. Thermophysical properties of fluids. II. Methane, ethane, propane, isobutane, and normal butane. *J. Phys. Chem. Ref. Data* **1987**, *16*, 577−798.
(87) Jorgensen, W. L.; Maxwell, D. S.; Tirado-Rives, J. Development and testing of the OPLS all-atom force fields on conformational energetics and properties of organic liquids. *J. Am. Chem. Soc.* **1996**, *118*, 11225−11236.
(88) Jorgensen, W. L.; Laird, E. R.; Nguyen, T. B.; Tirado-Rives, J. Monte Carlo simulations of pure liquid substituted benzenes with OPLS potential functions. *J. Comput. Chem.* **1993**, *14*, 206−215.
(89) Stewart, J. J. P. *MOPAC2012*; Stewart Computational Chemistry (SCC): Colorado Springs, CO, 2012; http://OpenMOPAC.net.
(90) Seidl, P. R.; Oliveira, J. C. S.; da Costa, L. M.; Stoyanov, S. R. A computational study on the steric effects of cyclic aliphatic moieties on the aggregation interactions in non-conventional petroleum constituents. *J. Phys. Org. Chem.* **2014**, DOI: 10.1002/poc.3329.
(91) Rudyk, S.; Husain, S.; Spirov, P. Supercritical extraction of crude oil by methanol- and ethanol-modified carbon dioxide. *J. Supercrit. Fluids* **2013**, *78*, 63−69.


DOI: 10.1021/ef502202q
*Energy Fuels* 2015, 29, 2853−2863